CrystEngComm

Accepted Manuscript

Volume 1 | Number 1 | Jan 2013 | Pages 1–100

CrystEngComm

www.rsc.org/crystengcomm

ROYAL SOCIETY OF CHEMISTRY

ROYAL SOCIETY OF CHEMISTRY

www.rsc.org/crystengcomm

Investigation on YF_3:Eu^{3+} architectures and their luminescent properties

Longxiang Yan, Wei Gao, Qinyan Han, Xiaoyi Li, Ruibo Wang, Chengyun Zhang, Mingdi Zhang, Linxiao Wang, Hairong Zheng*

School of Physics and Information Technology, Shaanxi Normal University, Xi'an 710062, China

*Corresponding author: Hairong Zheng

Email: hrzheng@snnu.edu.cn

Abstract: Well-dispersed YF_3:Eu^{3+} architectures with different morphologies are obtained via low temperature solid-state reaction process by tuning the fluoride source. With increase of the calcination temperature from 400°C to 1000°C, the products undergo an obvious matrix transformation from yttrium fluoride to yttrium oxide fluoride, and then yttrium oxide. The local symmetry of optical active Eu^{3+} ions decreases with increase of calcination temperature at lower calcination temperature region, and then keeps almost unchanged when the temperature is over 700°C. Different luminescent properties of the as-prepared YF_3:Eu^{3+} architectures and the products calcinated at different calcination temperatures are observed even for the samples with the same contents. The study may have special significance to the large-scale fabrication of other lanthanide fluoride luminescent materials.

Key words: yttrium fluoride; solid-state reaction; matrix transformation; local symmetry; luminescent property

1. Introduction

Lanthanide doped nano/micromaterials have attracted wide attention due to their prolific and potential applications in various fields of modern science such as solid state lasers[1], solar cells[2], photoswitching[3], and fluorescent labels[4]. Among them, fluoride nano/microcrystals have special advantages due to their high chemical stability, low toxicity, long luminescent lifetime and low optical phonon energy[5-8]. As to the fluoride materials,

Ln^{3+}-doped YF_3 has efficient light emissions and can have various morphologies by simple tuning of the synthetic conditions[9-11]. Up to now, many fabrication methods have been developed with different sizes and morphologies which include hydrothermal method[12-14] and solvothermal method[15-16], microemulsion[17], sol-gel method[18], ionic liquid based route[19], electrospining with fluorination technique[20], and double-crucible method[21]. However, most methods mentioned above need long reaction time, high reaction temperature and pressure. The addition of capping agents for size and shape control may result in additional impurities in the final results. Therefore, it is desirable to develop some low temperature synthetic techniques to fabricate large-scale and well-crystallized Ln^{3+}-doped YF_3 luminescent materials.

Because of the poor crystallinity of the product compared with other synthetic methods, low temperature synthetic routes have not been paid enough attention. Jia's group showed various morphologies of YF_3 by adjusting the reaction temperature and fluoride source[22]. Similar results were obtained by Mahalinggam's and Zhong's group through wet-chemical route[23-24]. Whereas, further investigation based on the products was rarely reported. It is known that oxide nano/submicrocrystals have better chemical stability and mechanical strength, but they usually have much higher phonon energy (larger than 500 cm^{-1}) comparing with fluoride ones. Oxyfluoride nano/submicrocrystals combine the advantages of both fluoride and oxide nano/submicrocrystals. They present better chemical and thermal stability than fluorides, and lower phonon energy than oxides[25]. Therefore, the investigation on the matrix transformation process and luminescent properties becomes necessary.

In this paper, we present a simple wet-chemical approach to synthesize $YF_3:Eu^{3+}$ architectures with two different morphologies at ambient pressure and low temperature without any additional catalysts, templates, or surfactant. The morphology, structure and the dependence of luminescent properties on morphology and treatment process are studied systematically for as-prepared $YF_3:Eu^{3+}$ samples and their calcinated products. The investigation on the synthesis approach and matrix transformation process could have valuable significance to the exploration of other fluoride luminescent materials.

2. Experimental Sections

2.1 Chemicals

All the chemicals used in the current study are analytic graded and used as received without further purification. Y_2O_3 and Eu_2O_3 (99.9%) was purchased from Sigma-Aldrich Chemicals Co.. NH_4F (96%), NaF (98%) were supplied by Sinopharm Chemical Reagent Co., Ltd. (China). $Ln(NO_3)_3$ (Ln = Y, Eu) was prepared by dissolving the corresponding oxide in dilute nitric acid at elevated temperature followed by evaporating the superfluous nitric acid. Deionized (DI) water was used throughout the experiments unless stated otherwise.

2.2 Preparation of YF_3:Eu^{3+} architectures

The wet-chemical method was employed for sample synthesis in current study. By taking the sample of YF_3:5.0%Eu^{3+} as an example, we illustrate the preparation procedure as follow. In a typical process, 1.9 mmol $Y(NO_3)_3$ and 0.1 mmol $Eu(NO_3)_3$ aqueous solution were added to 40 ml deionized water with stirring and heated to 75°C. Then the aqueous solution containing 0.257g of NaF (6.0 mmol) was introduced dropwise to the vigorously stirred solution. After additional agitation for 2 hours, the obtained white precipitates were collected and separated by centrifugation, washed with deionized water and ethanol, and finally dried at 70°C in air (denoted as **S1**). A similar synthesis procedure was employed to prepare the samples with NH_4F instead of NaF as the fluoride source, which were denoted as **S2**. The as-obtained YF_3:Eu^{3+} samples were calcinated at different temperatures for 1 hour in air, respectively.

2.3 Characterization

X-ray powder diffraction (XRD) measurements were performed on a Rigaku D/Max2550 diffractometer at a scanning rate of 8°min^{-1}, with graphite monochromatic Cu Kα irradiation (λ= 0.15406 nm). The morphology and composition of the samples were observed with JEOL 2100 transmission electron microscope (TEM) at 200 kV and scanning electron microscope (Bruker) equipped with an energy dispersive X-ray (EDX). The LabRam confocal microprobe Raman system (Jobin-Yvon) is used for luminescence collection and detection. A laser at 532 nm is employed as excitation sources during the fluorescence spectroscopic measurement. The powder sample for each measurement was weighed to ensure the same amount to be excited. All of the spectroscopic measurements are carried out at room temperature.

3. Results and discussion

3.1 Characterization of samples

Figure 1 shows the X-ray diffraction patterns (XRD) of the samples **S1** and **S2** prepared at different reaction conditions. The diffraction peaks of two samples agree well with orthorhombic phase YF_3 (JCPDS 70-1935). However, the diffraction intensity of sample **S1** is stronger and sharper than that of the sample **S2**, which illustrates a better crystallization in the sample **S1**. It is also noticed that relative intensity distribution of the diffraction peaks in the XRD pattern are different for two samples, reflecting different arrangement of $YF_3:Eu^{3+}$ architecture as presented in the insets of Figure 1. A nanospindle $YF_3:Eu^{3+}$ with about 900 nm in length and 300 nm in middle width is obtained when NaF is used as fluoride source. However, when the fluoride source NaF is replaced by NH_4F, the sample becomes a nanobundle for which the middle diameter is about 200 nm and the length is about 1 μm. These results suggest that the fluoride source plays an important role in the sample growth and affects the final morphology of $YF_3:Eu^{3+}$ particle.

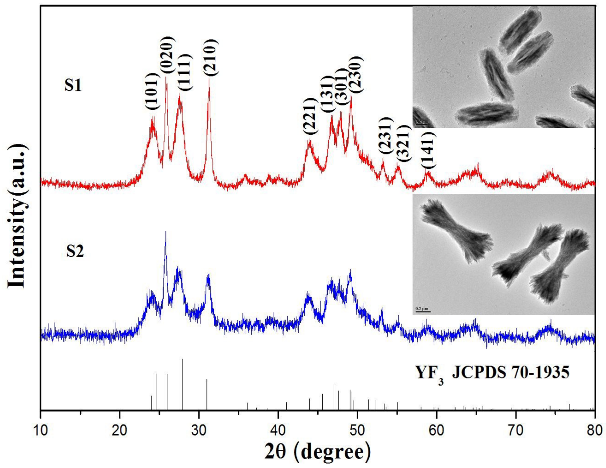

Fig. 1 XRD patterns of the spindle-like (**S1**) and bundle-like (**S2**) YF_3:5.0%Eu^{3+} sample powders. The insets are corresponding TEM images.

When the as-obtained YF_3: 5.0%Eu^{3+} particles are calcinated at different temperatures, the structure of the sample particles changes accordingly. Figure 2 presents XRD patterns of the samples calcinated at different temperatures. When the temperature is below 400°C, the YF_3 sample keeps orthorhombic phase but the diffraction peaks become sharper and stronger with temperature increase, showing a higher crystallinity when it is calcinated. However, a new peak begins to appear when the temperature goes to 500°C indicating a formation of partial oxidation in the sample. When the temperature reaches to 700°C, the sample changes to $Y_7O_6F_9$ and presents pure orthorhombic phase $Y_7O_6F_9$ (JCPDS 70-0867). Continuously increase the temperature to 800°C, the phase of rhombohedral YOF (JCPDS 71-2100) emerges, suggesting that YF_3 particles successfully transforms into yttrium oxyfluoride. Further increasing the temperature to 1000°C results in a rhombohedral phase Y_2O_3 (JCPDS 83-0927). Figure 2 also shows that the diffraction peaks become stronger and narrower with increase of the temperature, indicating the growth of crystalline particles with better crystallinity.

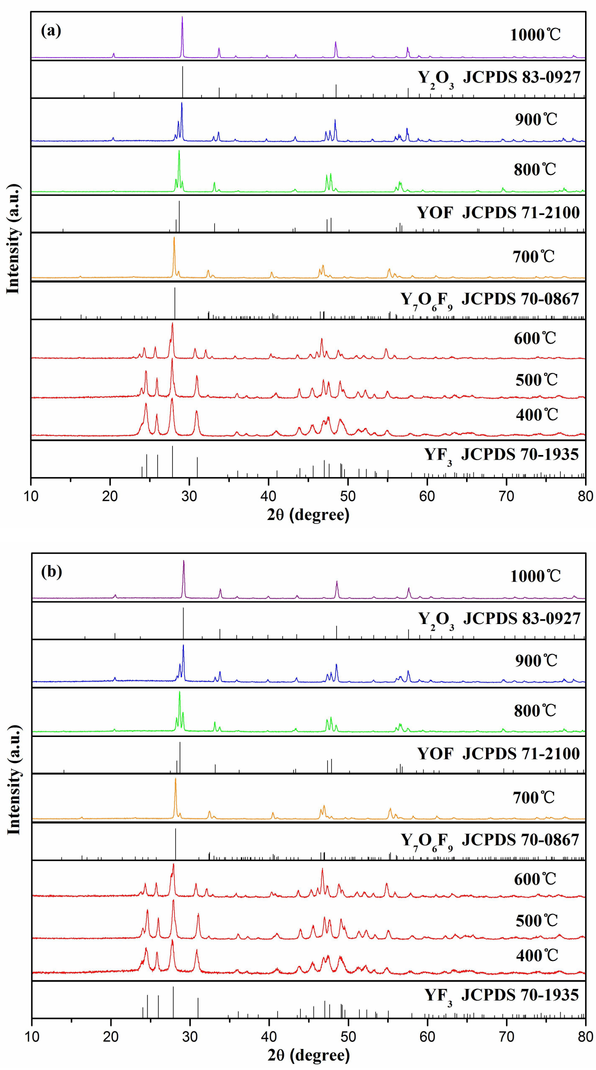

Fig. 2 XRD patterns of the spindle-like **S1** (a) and bundle-like **S2** (b) YF_3:5.0%Eu^{3+} sample powders calcinated at different temperatures for 1 hour.

The morphology and crystal structure of the samples are characterized with SEM. Figure 3 (a) and (a_1) present spindle-like and bundle-like YF_3:5.0%Eu^{3+} architectures that are uniform and well-dispersed. To understand the growth process of the samples, a solution-solid process[26-27] theory is necessary introduced. In this process, amorphous nuclei are formed immediately in the mixed aqueous solution under vigorous stirring. The newly formed nuclei have a very low growth rate at a low temperature in the early nucleation stage, which ensures a definite separation of nucleation and growth[28]. Then the amorphous nuclei turn into crystalline nanoparticles. With the reaction proceeding, the as-formed nanoparticles begin to aggregate in a certain way and undergo a further crystal growth and crystallization process to form different architectures. The formation of different morphologies for YF_3:5.0%Eu^{3+} samples could be attributed to the release of F^- ions which is necessay for the YF_3 formation[23] and the chemical potential of the reaction system[29]. Compared with fluoride source NaF, NH_4F is more soluble in water so that more F^- ions are readily available to combine with Y^{3+} ions. The difference in F^- ions concentration may lead to the different sizes of crystalline nanoparticles for different fluoride sources. Driven by a higher chemical potential, the nanoparticles with different sizes grow into one-dimensional spindle-like and bundle-like architectures.

Figure 3 (b) to (f) and Fig 3 (b_1) to (f_1) are SEM images of samples **S1** and **S2** calcinated at different temperatures. The morphology and size are basically preserved below 400°C. However, with further increase of the calcination temperature, all the samples begin to agglomerate, which is due to agglomerate and self-assembly process happening under the effect of oxygen that leads to the transformation from yttrium fluoride to yttrium oxyfluoride[24]. When the temperature reaches to 1000°C, there are enough energy and oxygen atoms for the formation of Y_2O_3 accompanied by a dissolution-recrystallization process[30].

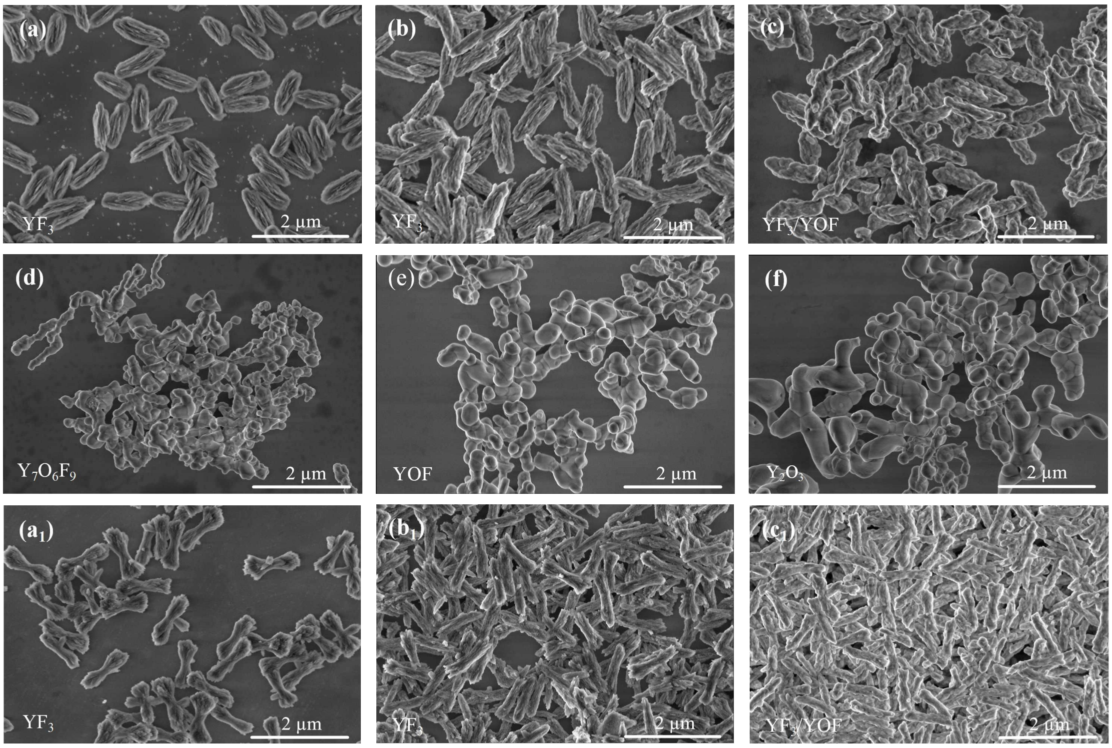

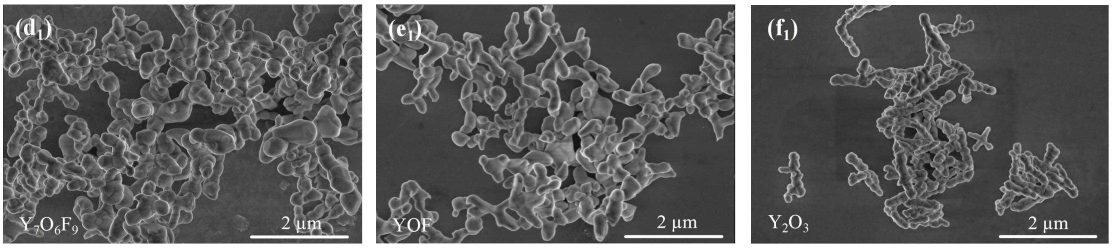

Fig. 3 SEM images of the spindle-like (a) to (f) and bundle-like (a_1) to (f_1) YF_3:5.0%Eu^{3+} sample powders calcinated at different temperatures for 1 hour. (b, b_1) 400°C, (c, c_1) 500°C, (d, d_1) 700°C, (e, e_1) 800°C, (f, f_1) 1000°C.

Due to similar electronic structures (S^2P^6) and dimension (0.90 Å and 0.95 Å), the Eu^{3+} ion can easily replace Y^{3+} ion and be effectively doped into YF_3 host lattice, which are proved by EDX and photoluminescence spectra. As shown in Figure 4, the EDX spectra confirm the existence of F, Y, and Eu in the YF_3:5.0%Eu^{3+} sample and the appearance of O element in the calcinated samples. The content of O element increases with the increase of calcination temperature, meanwhile the content of F element decreases gradually and finally gets vanished in the spectra at last. Thus the composition change of the product with calcination temperature is reflected with EDX spectra, which agrees with the XRD result as presented in Figure 2. In Figure 4, the peaks of element C and Al come from the conductive adhesive and sample holder, respectively.

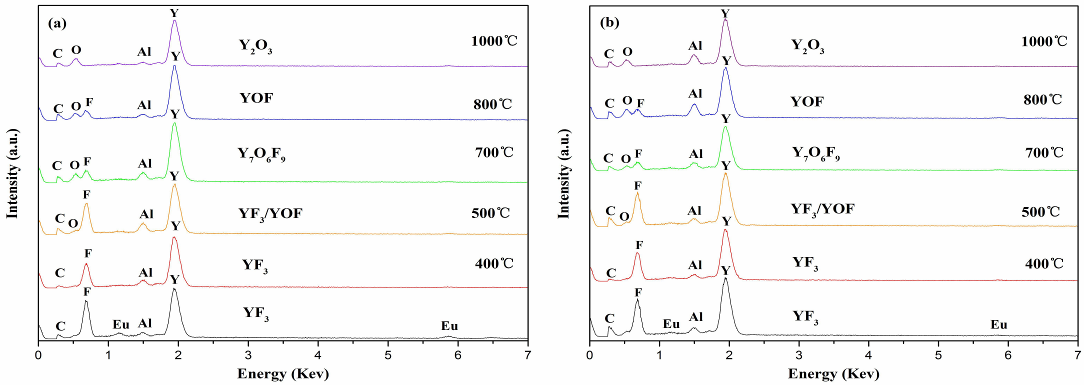

Fig. 4 EDX spectra of the spindle-like (a) and bundle-like (b) YF_3:5.0%Eu^{3+} sample powders and those calcinated at different temperatures for 1 hour.

3.2 Luminescent properties

YF_3 is an efficient host lattice for the luminescence emission of many optically active lanthanide ions[31-33]. Figure 5 are photoluminescence (PL) emission spectra of samples **S1** and **S2** under the excitation of 532 nm. Both samples present characteristic emissions of Eu^{3+} ions with similar profile but different emission intensities. The prominent emission bands locate at around 554 nm, 558 nm, 579 nm, 592 nm, 616 nm, 650 nm and 700 nm, which are assigned to the transitions of $^5D_1$-$^7F_2$, $^5D_1$-$^7F_3$, $^5D_0$-$^7F_0$, $^5D_0$-$^7F_1$, $^5D_0$-$^7F_2$, $^5D_0$-$^7F_3$ and $^5D_0$-$^7F_4$, respectively. It is easy to notice that the luminescence emission intensity of sample **S1** is stronger than that of sample **S2** due to better crystallinity of the sample **S1** as presented in Figure 1.

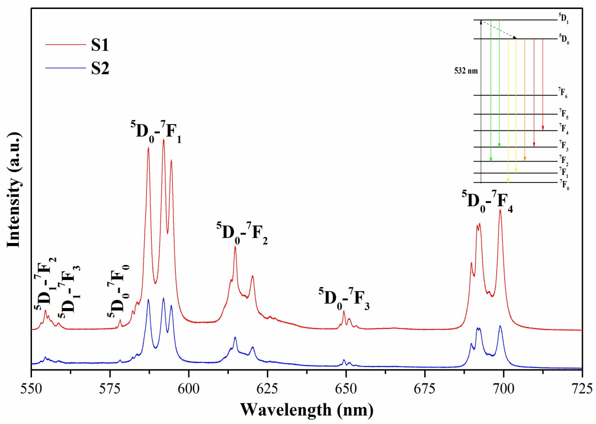

Fig. 5 Photoluminescence emission spectra of spindle-like (**S1**) and bundle-like (**S2**) YF_3:5.0%Eu^{3+} sample powders. The inset is schematic energy levels of Eu^{3+} and corresponding transitions related to the photoluminescence emissions.

Figure 6 shows the emission spectra of the samples **S1** and **S2** calcinated at different temperatures. The emission intensity of the sample increases significantly with the increase of calcination temperature. Insets of the figure present the corresponding intensity ratio (η) of $^5D_0$-$^7F_1$ to $^5D_0$-$^7F_2$ with different calcination temperatures. It can be seen that the η value decreases from around 0.90 to 0.70 as the calcination temperature increases to 500°C for both samples of **S1** and **S2**, and keeps at around 0.18 when the calcination temperature is higher than 700°C.

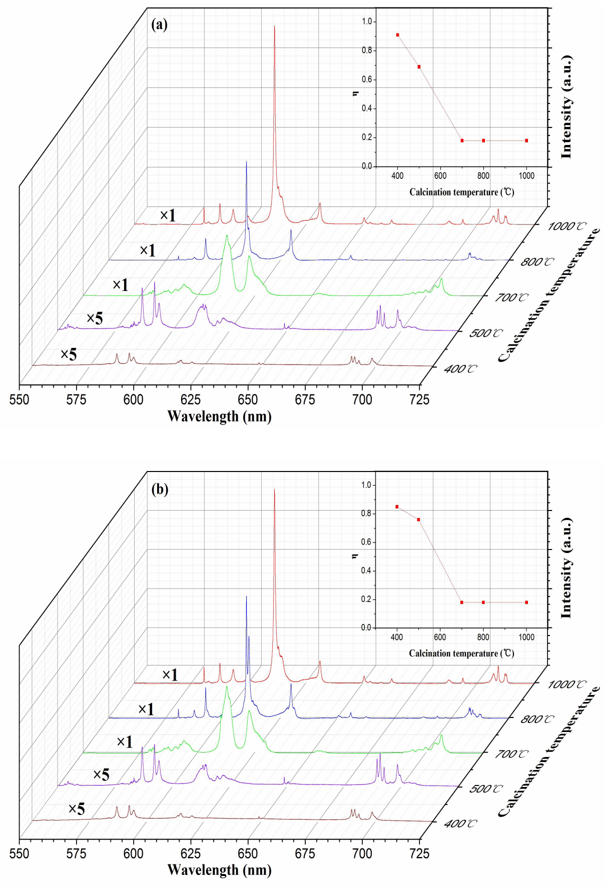

Fig. 6 Photoluminescence emission spectra of the sample **S1** (a) and **S2** (b) calcinated at different temperatures for 1 hour. Insets are corresponding intensity ratios (η) of $^5D_0$-$^7F_1$ to $^5D_0$-$^7F_2$ with different calcination temperatures.

It is well known that the intensity ratio (η) of $^5D_0$-$^7F_1$ to $^5D_0$-$^7F_2$ of Eu^{3+} strongly depends on the local symmetry. Therefore, Eu^{3+} ions are often used as probes to detect local environments in the matrix material. It is reported that the transition $^5D_0$-$^7F_1$ dominates in a site with inversion symmetry, while the $^5D_0$-$^7F_2$ is the strongest transition in a site without inversion symmetry[12,14,15]. In the emission spectra of samples **S1** and **S2**, the dominating emissions correspond to the magnetic dipole transition of $^5D_0$-$^7F_1$ and their η values are 2.03, 1.79, respectively, which indicates that Eu^{3+} ion locates in a site with inversion symmetry. After a calcination treatment, the spectra begin to split up. In the emission spectra of the samples calcinated at 400°C and 500°C, the intensity ratio decreases due to partial oxidation that causes the enhanced emission of electric dipole transition $^5D_0$-$^7F_2$. In the emission spectra of the samples calcinated at higher temperatures of 700°C, 800°C and 1000°C, $^5D_0$-$^7F_2$ transitions are much stronger than $^5D_0$-$^7F_1$ transitions, indicating Eu^{3+} ion locates in a site with less inversion symmetry, which suggests an obvious change of the local environment around Eu^{3+} ion. This observation on the local environment change agrees well with the matrix transformation process discussed in the previous section.

Conclusions

In summary, well-dispersed YF_3:Eu^{3+} architectures with two different morphologies are reported with facile low temperature solid-state method through changing fluoride source. Different crystal structure and contents of the sample are obtained by calcinating the sample at different temperatures. It is found that the morphology and crystallinity influence the luminescence properties significantly. The changeable matrix under different calcination temperatures leads to a tunable luminescent property. The green and low-cost synthesis approach could be useful for the exploration of new lanthanide fluoride materials.

Acknowledgement

This work is supported by the National Science Foundation of China (Grant No. 11174190 and 11304247), the Natural Science Foundation of Shaanxi Educational Committee (Grant No. 2013JK0627) and the Natural Science Basis Research Plan in Shaanxi Province of China (Grant No. 2013JM1008).

References

[1] M. H. Huang, S. Mao, H. Feick, H. Yan, Y. Wu, H. Kind, E. Weber, R. Russo and P. Yang, *Science*, 2001, **292**, 1897-1899.

[2] D. Chen, Y. Wang and M. Hong, *Nano. Energy*, 2012, **1**, 73-90.

[3] J. C. Boyer, C. J. Carling, B. D. Gates and N. R. Branda, *J. Am. Chem. Soc.*, 2010, **132**, 15766-15772.

[4] T. S. Yang, Y. Sun, Q. Liu, W. Feng, P. Y. Yang and F. Y. Li, *Biomaterials*, 2012, **33**, 3733-3742.

[5] L. Q. Xiong, T. S. Yang, Y. Yang, C. J. Xu and F. Y. Li, *Biomaterials*, 2010, **31**, 7078-7085.

[6] W. Feng, C. M. Han and F. Y. Li, *Adv. Mater.*, 2013, **25**, 5287-5303.

[7] Y. Liu, D. Tu, H. Zhu and X. *Chen, Chem. Soc. Rev.*, 2013, **42**, 6924-6958.

[8] F. Wang, Y. Han, C. S. Lim, Y. H. Lu, J. Wang, J. Xu, H. Y. Chen, C. Zhang, M. H. Hong and X. G. Liu, *Nature*, 2010,

463, 1061-1065.

[9] N. O. Nunez, M. Quintanilla, E. Cantelar, F. Cusso and M. Ocana, *J. Nanopart. Res.*, 2010, **12**, 2553-2565.

[10] C. Peng, C. Li, G. Li, S. Li and J. Lin, *Dalton Trans.*, 2012, **41**, 8660-8668.

[11] C. X. Li, P. A. Ma, P. P. Yang, Z. H. Xu, G. G. Li, D. M. Yang, C. Peng and J. Lin, *CrystEngComm*, 2011, **13**, 1003-1013.

[12] F. Tao, Z. Wang, L. Yao, W. Cai and X. Li, *J. Phys. Chem. C*, 2007, **111**, 3241-3245.

[13] M. Wang, Q. L. Huang, H. X. Zhong, X. T. Chen, Z. L. Xue and X. Z. You, Cryst. Growth Des., 2007, **7**, 2106-2111.

[14] M. F. Zhang, H. Fan, B. J. Xi, X. Y. Wang, C. Dong and Y. T. Qian, *J. Phys. Chem. C*, 2007, **111**, 6652-6657.

[15] S. Wang, H. Xu, X. Chen, S. Zhong, J. Jiang, Y. Huang, S. Wang and R. Xu, *J. Cryst. Growth*, 2008, **310**, 4697-4700.

[16] J. Zhao, M. Zhu, L. Mu, Z. Yang, L. Wang, L. Gu and Y. Hu, *J. Colloid and Interface Science*, 2014, **436**, 171-178.

[17] G. Wang, W. Qin, J. Zhang, J. Zhang, Y. Wang, C. Cao, L. Wang, G. Wei, P. Zhu and R. Kim, *J. Phys. Chem. C*, 2008, **112**, 12161-12167.

[18] K. Banger, Y. Yamashita, K. Mori, R. Peterson, T. Leedham, J. Rickard and H. Sirringhaus, *Nat. Mater.*, 2010, **10**, 45-50.

[19] N. O. Nunez and M. Ocana, *Nanotechnology*, 2007, **18**, 455606.

[20] D. Li, J. Wang, X. Dong, W. Yu and G. Liu, *J. Mater. Sci.*, 2013, **48**, 5930-5937.

[21] D. Li, X. Dong, W. Yu, J. Wang and G. Liu, *J. Nanopart. Res.*, 2013, **15**(6), 1-10.

[22] G. Jia, C. M. Huang, C. Z. Wang, J. J. Jiang, S. Li and S. W. Ding, *CrystEngComm.*, 2012, **14**, 4425-4430.

[23] S. Sarkar and V. Mahalingam, *CrystEngComm.*, 2013, **15**, 5750-5755.

[24] H. Fang, H. L. Xu, L. J. Bai, D. D. Guo and S. L. Zhong, *Rare Met.*, 2014, **33**, 604-607.

[25] G. Chai, G. Dong, J. Q, Q. Zhang and Z. Yang, *SCIENTIFIC REPORTS*, 2013, **3**, 1598.

[26] X. Wang and Y. D. Li, *J. Am. Chem. Soc.*, 2002, **124**, 2880-2881.

[27] G. Xi, K. Xiong, Q. Zhao, R. Zhang, H. Zhang and Y. Qian, *Cryst. Growth Des.*, 2006, **6**, 577-582.

[28] B. Shao, Q. Zhao, Y. Jia, W. Lv, M. Jiao, W. Lü and H. You, *J. Mater. Chem. C*, 2014, **2**, 7666-7673.

[29] Z. A. Peng and X. Peng, *J. Am. Chem. Soc.*, 2001, **123**, 1389-1395.

[30] G. Dong, B. Chen, X. Xiao, G. Chai, Q. Liang, M. Peng and J. Qiu, *Nanoscale*, 2012, **4**, 4658-4666.

[31] R. X. Yan and Y. D. Li, *Adv. Funct. Mater.*, 2005, **15**, 763-770.

[32] Z. F, X. Cui, S. Cui, X. Qi, S. Zhou, S. Zhang and J. H. Jeong, *CrystEngComm.*, 2012, **14**, 3915-3922.

[33] F. N. Sayed, V. Grover, S. V. Godbole and A. K. Tyagi, *RSC. Advances*, 2012, **2**, 1161-1167.

Table of Contens Entry

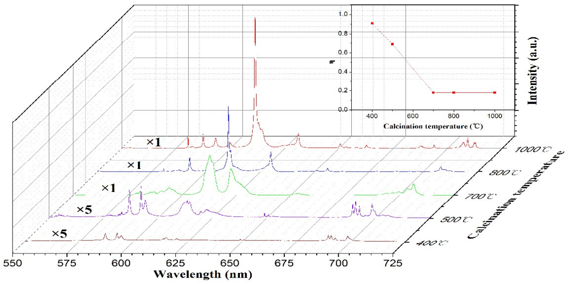

The changeable matrix under different calcination temperatures leads to a tunable luminescent property.